University of Montana

ScholarWorks at University of Montana

Numerical Terradynamic Simulation Group Publications

Numerical Terradynamic Simulation Group

Satellite-based model detection of recent climate-driven changes in northern high-latitude vegetation productivity

Ke Zhang
The University of Montana

John S. Kimball
University of Montana - Missoula

E. H. Hogg

Maosheng Zhao

Walter C. Oechel

See next page for additional authors

Follow this and additional works at: https://scholarworks.umt.edu/ntsg_pubs

Let us know how access to this document benefits you.

Recommended Citation

Zhang, K., J. S. Kimball, E. H. Hogg, M. Zhao, W. C. Oechel, J. J. Cassano, and S. W. Running (2008), Satellite-based model detection of recent climate-driven changes in northern high-latitude vegetation productivity, J. Geophys. Res., 113, G03033, doi:10.1029/2007JG000621

Authors

Ke Zhang, John S. Kimball, E. H. Hogg, Maosheng Zhao, Walter C. Oechel, John Cassano, and Steven W. Running

Satellite-based model detection of recent climate-driven changes in northern high-latitude vegetation productivity

Ke Zhang,[1,2] John S. Kimball,[1,2] E. H. Hogg,[3] Maosheng Zhao,[2] Walter C. Oechel,[4] John J. Cassano,[5] and Steven W. Running[2]

[1]   We applied a satellite remote sensing based production efficiency model (PEM) using an integrated AVHRR and MODIS FPAR/LAI time series with a regionally corrected NCEP/NCAR reanalysis daily surface meteorology and NASA/GEWEX Surface Radiation Budget shortwave solar radiation inputs to assess annual terrestrial net primary productivity (NPP) for the pan-Arctic basin and Alaska from 1983 to 2005. Our results show that low temperature constraints on Boreal-Arctic NPP are decreasing by 0.43% per year ($P < 0.001$), whereas a positive trend in vegetation moisture constraints of 0.49% per year ($P = 0.04$) are offsetting the potential benefits of longer growing seasons and contributing to recent disturbances in NPP. The PEM simulations of NPP seasonality, annual anomalies and trends are similar to stand inventory network measurements of boreal aspen stem growth ($r = 0.56$; $P = 0.007$) and atmospheric CO_2 measurement based estimates of the timing of growing season onset ($r = 0.78$; $P < 0.001$). Our results indicate that summer drought led to marked NPP decreases in much of the boreal forest region after the late-1990s. However, seasonal low temperatures are still a dominant limitation on regional NPP. Despite recent drought events, mean annual NPP for the pan-Arctic region showed a positive growth trend of 0.34% per year (20.27 TgC/a; $P = 0.002$) from 1983 to 2005. Drought induced NPP decreases may become more frequent and widespread as regional ecosystems adjust to a warmer, drier atmosphere, though the occurrence and severity of drought events will depend on future patterns of plant-available moisture.

1. Introduction

[2]   Seasonal and annual variations in terrestrial photosynthesis and net primary production (NPP) strongly impact the annual growth rate of atmospheric CO_2, which has been increasing in concentration through anthropogenic emissions of fossil fuels and is considered to be a major cause of global warming [*Arctic Climate Impact Assessment (ACIA)*, 2004; *Angert et al.*, 2005]. Boreal forest and arctic tundra biomes of the pan-Arctic basin and Alaska are the main components of northern high latitude ($>50°N$) ecosystems and encompass 30% of the combined North American and Eurasian landmass [*Kimball et al.*, 2006a]. The biomes in this region contain up to 40% of the global soil organic carbon reservoir [*Saugier et al.*, 2001; *Lal and Kimble*, 2000] and an improved assessment of recent changes in NPP for the region is vital for understanding the terrestrial carbon cycle response to global climate change.

[3]   Recent warming trends may be enhancing carbon sequestration in this region by increasing vegetation growth. However, warming may also be enhancing carbon losses by increasing vegetation stress, soil decomposition, carbon volatilization, and respiration processes [*Oechel et al.*, 1995, 2000; *Stocks et al.*, 2002; *Barber et al.*, 2000]. Ecosystem responses to warming trends include thawing permafrost and increases in soil active layer depths, advances in the timing and length of seasonal growing seasons, increased vegetation structure and growth, and alteration of land-atmosphere CO_2 exchange [*Oelke et al.*, 2004; *Sturm et al.*, 2001; *Euskirchen et al.*, 2006]. Earlier studies have shown evidence of an increasing trend in vegetation photosynthetic activity and NPP for the northern terrestrial

[1]Flathead Lake Biological Station, University of Montana, Polson, Montana, USA.
[2]Numerical Terradynamic Simulation Group, Department of Ecosystem and Conservation Sciences, University of Montana, Missoula, Montana, USA.
[3]Northern Forestry Centre, Canadian Forest Service, Natural Resources Canada, Edmonton, Alberta, Canada.
[4]Global Change Research Group, Biology Department, San Diego State University, San Diego, California, USA.
[5]Cooperative Institute for Research in Environmental Sciences and Department of Atmospheric and Oceanic Sciences, University of Colorado, Boulder, Colorado, USA.
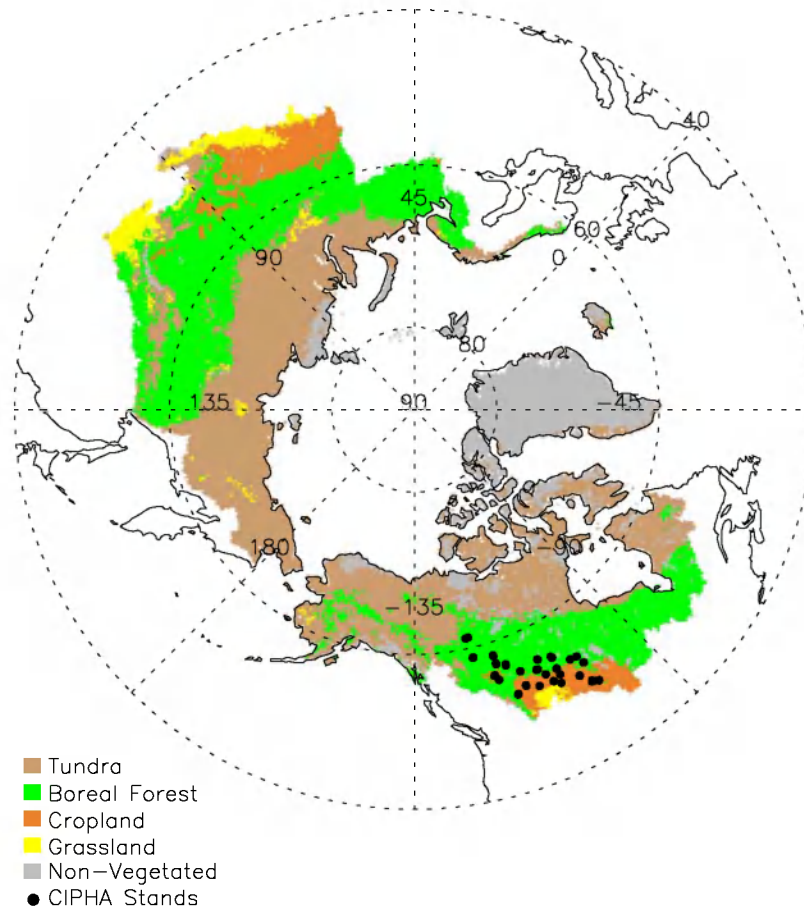
Figure 1. Map of aggregated land cover for the pan-Arctic basin and Alaska domain derived from the NASA IGBP-MODIS global land cover classification; the location of CIPHA stands in western Canada are also shown.

latitudes during the 1980s and 1990s, including analyses of atmospheric CO_2 anomalies [*Keeling et al.*, 1996; *Randerson et al.*, 1999; *McDonald et al.*, 2004], satellite normalized difference vegetation index (NDVI) derived greening trends [*Myneni et al.*, 1997a; *Zhou et al.*, 2001; *Slayback et al.*, 2003], production efficiency model based NPP calculations [*Nemani et al.*, 2003; *Zhao et al.*, 2006; *Kimball et al.*, 2006a; *Zhang et al.*, 2007a], and global vegetation and ecosystem process model simulations of the terrestrial carbon cycle [*McGuire et al.*, 2001; *Kimball et al.*, 2006b]. However, more recent atmospheric CO_2 anomalies [*Angert et al.*, 2005], satellite NDVI records [*Goetz et al.*, 2005], and ground-based observations [*Schindler and Donahue*, 2006; *Hogg et al.*, 2008] indicate a general decrease in vegetation productivity for North American boreal forests since the late-1990s, and may reflect the occurrence of widespread drought [*Hogg et al.*, 2005, 2008].

[4] In a previous study [*Zhang et al.*, 2007a] we showed that the accuracy of NPP simulations from the MOD17A2/A3 Production Efficiency Model (PEM) was strongly limited over the northern high latitudes by large uncertainties in daily surface meteorological inputs from ECMWF ERA-40 and NCEP/NCAR reanalysis (NNR) products. Regional corrections of PEM based NPP using an uncertainty and sensitivity analysis method produced more reliable estimations of annual NPP and also confirmed a generally positive

trend in regional productivity from 1982 to 2000. In this study, we further refined meteorological inputs to the PEM by reducing large uncertainties in solar radiation inputs using the NASA/GEWEX Surface Radiation Budget (SRB) product and correcting reanalysis air temperature and humidity inputs using information from the surface weather station network. We also extended the satellite based NPP record through 2005 to assess the terrestrial productivity response to a continuing pattern of global warming and recent (post-2000) record warm, dry conditions across the pan-Arctic. We also compare PEM derived NPP results with boreal aspen stem growth anomalies for 72 stands distributed across west-central Canada to determine the consistency between relatively coarse scale satellite remote sensing and stand level measurements of recent changes in vegetation productivity. The primary objective of this paper is to quantify the spatial patterns, temporal anomalies, and recent trends in terrestrial NPP for the pan-Arctic domain and uncover the driving forces of these changes.

2. Data Sets and Methods

2.1. Study Area

[5] The domain of this investigation encompasses the pan-Arctic basin and Alaska (Figure 1) [*Zhang et al.*, 2007a]. To study climate change effects on major biomes

within the domain, we first calculated annual NPP and other related parameters using the standard International Geosphere-Biosphere Programme (IGBP) 17-class MODIS global land cover classification [*Friedl et al.*, 2002] and then aggregated the results into the four major regional vegetation types: tundra, boreal forest, cropland and grassland (Figure 1) to assess productivity changes among the major biomes. In this study, we only focus on the two dominant unmanaged biomes: tundra and boreal forest.

2.2. NPP and Climatic Constraints Calculations

2.2.1. Satellite Production Efficiency Model Logic

[6] A biome-specific Production Efficiency Model (hereinafter, PEM) based on the MODIS MOD17A2/A3 algorithms [*Running et al.*, 2000, 2004; *Heinsch et al.*, 2003; *Nemani et al.*, 2003; *Zhao et al.*, 2008] was used to calculate gross primary production (GPP) and net primary production (NPP) for all vegetated grid cells at 25-km spatial resolution across the pan-Arctic domain. The model has undergone several revisions in response to extensive, ongoing calibration, and verification studies using biophysical information from regional station networks, including boreal and arctic landscapes [e.g., *Turner et al.*, 2003, 2005; *Zhao et al.*, 2005, 2006; *Heinsch et al.*, 2006; *Zhao et al.*, 2008]. The model is driven by satellite-derived land cover, fractional photosynthetically active radiation (FPAR), leaf area index (LAI) and daily surface meteorology including incident solar radiation (SW_{rad}), minimum and average daily air temperatures (T_{min} and T_{avg}), and daylight vapor pressure deficit (*VPD*). In this study, *VPD* is calculated from T_{avg} and mean daily atmospheric vapor pressure (e_a). Therefore, the actual PEM daily climate drivers include SW_{rad}, T_{min}, T_{avg} and e_a. GPP (g C m^{-2}) was derived on a daily basis as [*Running et al.*, 2000, 2004; *Heinsch et al.*, 2003; *Nemani et al.*, 2003]:

$$GPP = \varepsilon \cdot FPAR \cdot PAR \qquad (1)$$

$$\varepsilon = \varepsilon_{max} \cdot T_f \cdot VPD_f \qquad (2)$$

where ε is a light use efficiency parameter (g C MJ^{-1}) for the conversion of photosynthetically active radiation (PAR, MJ m^{-2}) to GPP, where PAR is assumed to represent 45% of incident solar radiation; ε_{max} is the potential maximum ε under optimal environmental conditions; T_f is a scalar that defines reductions in photosynthesis under low temperatures, while VPD_f is a scalar that defines similar reductions under suboptimal *VPD* and associated daytime water stress conditions. Both T_f and VPD_f are defined from T_{min} and *VPD* using simple photosynthetic response curves. NPP (g C m^{-2}) is derived on an annual basis as the difference between the annual summation of daily GPP and autotrophic growth and maintenance respiration:

$$NPP = \sum_{1}^{365} (GPP - R_{m\_lr}) - (R_{m\_w} + R_g) \qquad (3)$$

where R_{m_lr} is the daily maintenance respiration of leaves and fine roots; R_{m_w} represents the annual maintenance respiration from live wood; and R_g represents annual growth respiration. In this study, we defined the difference between daily GPP and R_{m_lr} as daily NPP. The characteristic response curves for calculating these parameters vary

according to the major biomes as defined by a Biome Properties Look-Up Table (BPLUT), which was developed from stand level ecophysiological studies [*White et al.*, 2000] and adjusted for the effects of regional meteorological and satellite-based FPAR/LAI data sets [*Running et al.*, 2000; *Zhao et al.*, 2005].

2.2.2. Climatic Constraints to PEM Based NPP

[7] To quantify the effects of low-temperature and moisture constraints to NPP, we defined a low-temperature stress index (I_t), and a moisture stress index (I_m):

$$I_t = 1 - T_f \qquad (4)$$

$$I_m = 1 - VPD_f \qquad (5)$$

The I_t and I_m parameters are dimensionless, ranging from 0 to 1 with increasing low-temperature and moisture constraints to GPP and NPP. We calculated potential NPP ($NPP_{Potential}$) under non limiting atmospheric conditions by removing both low-temperature and moisture constraints to the PEM calculations. We then calculated NPP using only moisture (NPP_M) and low-temperature (NPP_T) constraints, respectively. Finally, we determined the proportional (%) losses of potential NPP due to moisture ($\delta loss_M$) and low-temperature ($\delta loss_T$) constraints according to the following definitions:

$$\delta loss_M = \frac{NPP_{Potential} - NPP_M}{NPP_{Potential}} \times 100 \qquad (6)$$

$$\delta loss_T = \frac{NPP_{Potential} - NPP_T}{NPP_{Potential}} \times 100 \qquad (7)$$

[8] To verify changes in moisture availability for the domain, a simple climate moisture index (CMI) [*Hogg*, 1997; *Hogg et al.*, 2002, 2005, 2008] was computed as the difference between annual precipitation (P) and potential evapotranspiration (PET), where PET was calculated using a simplified Penman-Monteith approach [*Hogg*, 1997]. The CMI was derived on a 12-month period basis ending on 31 July of each given year from 1974 to 2005 using regional weather station observations of daily air temperature and precipitation provided by the NCDC CSB Global Surface Summary of the Day. The total number of NCDC CSB stations used to compute the CMI varied annually and ranged from 2053 to 2924 stations per year for the domain.

2.2.3. PEM Based Timing of Growing Season Onset

[9] We used the daily NPP series to derive annual growing season onset as the initial timing of positive daily NPP values for five out of seven consecutive days. We compared these results with the timing of the spring drawdown of atmospheric CO_2 concentrations [*Zhang et al.*, 2007b] derived from NOAA GMD monitoring stations across the pan-Arctic region (>50°N), including BRW (71°N), ALT (82°N), MBC (76°N), STM (66°N), CBA (55°N), ICE (63°N), SHM(52°N), SUM (72°N), and ZEP (79°N) stations [*GLOBALVIEW-CO₂*, 2006], to assess relative agreement between the satellite record and atmospheric CO_2 concentrations regarding recent trends and annual anomalies in northern growing season dynamics with regional warming. The average of the nine stations' mean monthly records were normalized as the difference between monthly and mean annual CO_2 concentrations for each year.

The timing of the spring 0-ppm crossing dates represents the X-intercept of the normalized monthly CO_2 transition from positive (winter) to negative (summer) conditions and is an indication of the seasonal timing of vegetation photosynthetic activity [*Keeling et al.*, 1996; *Randerson et al.*, 1999]. Previous studies have shown that the seasonal atmospheric CO_2 cycle at high northern latitudes is dominated largely by northern terrestrial ecosystems, with minimal impacts from ocean exchange, fossil fuel emissions, and tropical biomass burning [*Randerson et al.*, 1999; *Heimann et al.*, 1998; *Erickson et al.*, 1996].

2.3. Satellite FPAR/LAI Inputs

[10] In this study, we used satellite-derived vegetation properties including monthly FPAR and LAI from the NOAA AVHRR PAL 16-km resolution data set [*Myneni et al.*, 1997b] and 8-d FPAR and LAI from the NASA MODIS MOD15 1-km resolution data set [*Myneni et al.*, 2002]. The AVHRR PAL FPAR/LAI data are only available from 1982 to 2000, while the MODIS MOD15 FPAR/LAI data are ongoing and available since 2000. Because the NASA/GEWEX SRB shortwave solar radiation data are only available from 1983 to 2005, we chose 1983–2005 as our study period. A NASA Global Inventory Modeling and Mapping Studies (NASA GIMMS) NDVI product has made some improvements over the AVHRR PAL product and is currently available at 8-km resolution [*Pinzon et al.*, 2004]. However, there is currently no alternative GIMMS FPAR/LAI product with similar spatial resolution to the 16-km PAL data set for the study period.

2.3.1. Integration of AVHRR-MODIS FPAR/LAI Time Series

[11] To produce a continuous time series estimation of annual NPP from 1983 to 2005, we first employed a pixel-wise linear regression method to combine the two FPAR/LAI series into a single, continuous record, and then derived the long-term NPP record using the integrated AVHRR-MODIS FPAR/LAI series.

[12] The AVHRR PAL FPAR/LAI data are based on a monthly maximum value compositing of AVHRR spectral reflectance data to mitigate cloud cover, smoke, and other atmospheric aerosol contamination effects. To be consistent with the spatial resolution of the AVHRR PAL FPAR/LAI data, the 8-d 1-km MODIS FPAR/LAI data were first interpolated to a daily time step by removing cloud contamination and snow effects indicated by the MOD15A2 QC fields [*Zhao et al.*, 2005], followed by temporal linear interpolation of adjacent 8-d values to a daily time step, and spatial aggregation to a 16-km resolution by averaging the FPAR/LAI values of the dominant land cover class. The following procedures were then used to combine the two series: (1) derive monthly maximum values of MODIS FPAR/LAI for each pixel for 2000; (2) regress monthly MODIS FPAR/LAI on corresponding AVHRR FPAR/LAI for the overlapping period in 2000 using simple linear regression on a pixel-by-pixel basis; (3) use the resulting regression equations to adjust the AVHRR FPAR/LAI time series and compute an integrated AVHRR-MODIS FPAR/LAI monthly time series from 1983 to 2005. Although alternate regressions based on regional groupings by land cover type would increase the sample size for the linear regressions, this approach would not account for the con-

siderable spatial variation in the relationships between AVHRR and MODIS FPAR/LAI series, limiting the accuracy and reliability of this approach. The corrected monthly AVHRR PAL FPAR/LAI data were then resampled to a daily time step by temporal linear interpolation of adjacent monthly values. The daily linear interpolation approach used for this investigation is a relatively simple, but effective means for producing a daily FPAR and LAI time series for PEM simulations and has been used extensively for global vegetation analyses of the AVHRR Pathfinder series [e.g., *Kimball et al.*, 2006a; *Zhang et al.*, 2007a]. Finally, the combined data were reprojected to the 25 km polar EASE-grid format using a nearest-neighbor resampling scheme.

[13] There are three primary justifications for the above integration methods. First, the two products reflect quasi-simultaneous satellite observations of the same objects and show strong, positive correlations for most pixels. Although the observations were acquired from different sensors, similar physical mechanisms and models [*Myneni et al.*, 1997b, 2002] were used to produce each FPAR/LAI series. Second, the simple linear regression method is a global unbiased method which guarantees a reasonable error distribution and simplifies the evaluation of errors. Finally, the simple linear regression only involves linear transformation of the AVHRR FPAR/LAI time series, which conserves the same general trend as the original data series.

2.3.2. Validation of the Integrated FPAR/LAI Time Series

[14] To verify the consistency of our results, we compared the corrected monthly AVHRR FPAR/LAI series with corresponding MODIS FPAR/LAI values for 2000 by analyzing the error distribution and correlation results. In the validation procedure, we regarded the MODIS FPAR/LAI time series as "truth," while acknowledging that while MODIS has improved precision over AVHRR, there is no truly error free FPAR/LAI data set. Error from the validation procedure is defined as the estimated value, i.e., the corrected AVHRR FPAR/LAI, minus the true value, i.e., the MODIS FPAR/LAI. The mean ($\bar{\varepsilon}$), median (M_ε), standard deviation (i.e., standard error, s_ε), first quartile (Q_1), and third quartile (Q_3) of the error distribution are used to assess performance of the above methods. The mean absolute error (*MAE*) was also calculated to describe the spread of error. The relative error (δ), defined as the ratio of the absolute value of mean error to the mean absolute value of the observations, was used to show the relative magnitude of the errors, while the Pearson simple correlation coefficient was used to evaluate the strength of the relationships. We also evaluated the spatial distribution of errors.

[15] To evaluate the potential propagation of errors from integrated FPAR/LAI inputs on PEM based NPP calculations, we calculated 95% confidence intervals for estimated NPP before 2000. Due to the normal distributions of the errors for both LAI and FPAR, and the strong association between these variables, we assume that the errors for both LAI and FPAR have similar normal distributions. By adding and/or subtracting one standard error to LAI and FPAR inputs in combination and individually, we established 95% confidence intervals for the resulting PEM calculations.

[16] To assess the role of the historical FPAR/LAI record in determining the observed interannual variation in NPP

and associated sensitivity of PEM calculations to the AVHRR-MODIS integrated FPAR/LAI series, we conducted a sensitivity analysis by calculating NPP over the 23-year time series using a constant, average seasonal FPAR/LAI time series (i.e., the 23-year means) on a pixel-by-pixel basis. We then assessed differences between these results and the NPP series derived from the historical FPAR/LAI record.

2.4. Meteorological Inputs to the PEM

[17] We chose the National Centers for Environmental Prediction-National Center for Atmospheric Research (NCEP-NCAR) Reanalysis (NNR) [*Kalnay et al.*, 1996; *Kistler et al.*, 2001] Surface Flux product to provide daily meteorological inputs to the PEM. The NNR is provided four times per day in a global Gaussian grid (T62, 192 × 94 points) format with approximately $1.9° × 1.875°$ spatial resolution. The extracted data include surface air pressure, 2-m specific humidity, average air temperature, and extreme temperatures. The e_a term used to derive daylight *VPD* was calculated from NNR specific humidity and surface pressure information. Previous studies [*Zhao et al.*, 2006; *Zhang et al.*, 2007a] have shown that reanalysis meteorological data sets including the NNR introduce considerable uncertainty into PEM based NPP calculations. Due to large uncertainties in SW_{rad} from the NNR, we derived SW_{rad} from the NASA World Climate Research Programme/Global Energy and Water-Cycle Experiment (WCRP/GEWEX) Surface Radiation Budget (SRB) Project (http://eosweb.larc.nasa.gov/PRODOCS/srb/table_srb.html) data set. Due to the relative high quality of the SRB solar radiation product [*Gupta et al.*, 2001] and lack of direct solar radiation measurements in the region, we adopted the product without further corrections.

2.4.1. Correction of NNR Daily Surface Meteorology

[18] To reduce uncertainties in NNR inputs to the PEM, we applied a systematic correction of regional bias in the reanalysis daily surface meteorology through a local sample area correction method using surface observations of daily minimum and mean surface air temperatures and dew points from 1983 to 2005 for 6164 weather stations distributed across the pan-Arctic domain following *Zhang et al.* [2007a]. The following approach is used to correct NNR daily meteorological data (T_{min}, T_{avg}, and e_a): (1) interpolate NNR daily meteorological data for each WMO ground station using an inverse distance squared method; (2) subtract the interpolated NNR data from corresponding surface observations for each station and define the differences as correction terms; (3) select the nearest four stations for each NNR pixel within the domain, calculate the mean correction terms using the inverse distance squared method, and add the correction terms to the original NNR meteorological data.

2.4.2. Validation of Daily Meteorological Inputs

[19] To verify the quality of solar radiation inputs, we compared both NNR and SRB solar radiation data with daily solar radiation observations from 17 sites distributed across Alaska from 1983 to 1990. These data were obtained from the National Solar Radiation Data Base (NSRDB; http://rredc.nrel.gov/solar/old_data/nsrdb/), whereas the same validation procedures in section 2.3.2 were applied to assess product accuracy. Because of the extremely sparse

regional observation network for solar radiation, we didn't inspect the spatial distribution of errors in the radiation products; instead, we analyzed the temporal variation of errors using a one-way ANOVA.

[20] To verify the accuracy of the corrections, we calculated the interpolated meteorological variables for each station location using the corrected NNR. We then applied the same validation procedures in section 2.3.2 to analyze the resulting meteorological error distributions. In addition, we analyzed both temporal and spatial distributions of errors in the corrected NNR daily meteorological inputs.

2.4.3. Sensitivity of PEM NPP to Meteorological Inputs

[21] To verify corrected NNR and SRB inputs and quantify the propagation of associated errors in the NPP calculations, we estimated respective mean errors from three PEM NPP series derived from: (1) corrected NNR and SRB meteorology inputs; (2) corrected NNR T_{avg}, T_{min} and e_a, and NNR SW_{rad} inputs; and (3) NNR T_{avg}, T_{min}, e_a, and SW_{rad} inputs, where model results were assessed using the sensitivity analysis procedures of *Zhang et al.* [2007a]. The S-N-K ANOVA was then used to test the significance of error differences among the three PEM derived NPP series.

2.5. Comparison Between PEM and Stand Inventory Records

[22] The Climate Impacts on Productivity and Health of Aspen (CIPHA) study was initiated by the Canadian Forest Service (CFS) of Natural Resources Canada, and Environment Canada [*Hogg et al.*, 2005] to conduct tree ring analyses to examine the cause and magnitude of interannual variation in boreal aspen growth in western Canada (1800 km × 500 km area); CIPHA includes a regional network of long-term research plots in 72 aspen stands (Figure 1) distributed across the region. Tree ring analysis was conducted on samples at 1.3m height collected in fall 2000, and the chronologies were updated to include growth from 2001 to 2004 using the results from a second sampling in fall 2004.

[23] We compared the CIPHA mean aspen stem growth records, expressed as annual increments in stem cross-sectional area [*Hogg et al.*, 2005], from the 72 site locations with PEM derived mean NPP anomalies of the overlying grid cells to assess relative consistency between the coarse resolution satellite record and stand level measurements of recent changes in vegetation productivity. First, we removed cells classified as cropland or grassland instead of boreal forest to mitigate land cover misclassification effects between stand inventory and overlying satellite NPP results. The remaining NPP series were then weighted by the number of stands in each grid cell to derive the spatially averaged PEM based NPP series.

3. Results

3.1. Assessment of Meteorological and FPAR/LAI Inputs

[24] The summary of error distributions for the original and corrected NNR meteorological inputs (T_{avg}, T_{min}, and e_a) relative to daily surface weather station network observations are shown in Table 1. The error distributions of the combined AVHRR-MODIS FPAR/LAI series, and NNR

Table 1. Comparison of Accuracy in the Original and Corrected NNR Climate Data, NNR Solar Radiation, NASA/GEWEX SRB Solar Radiation, and Integrated Satellite FPAR/LAI Time Series[a]

Variables		$\bar{\varepsilon}$	s_{ε}	Q_1	M_{ε}	Q_3	MAE	δ	Correlation Coefficient
					Error Distribution				
T_{avg} (°C)	O[b]	−1.216	1.963	−2.038	−0.968	−0.072	1.640	31.62%	0.92
	C[c]	−0.030	0.857	−0.290	0.001	0.260	0.485	0.79%	0.99
T_{min} (°C)	O	−0.547	2.403	−1.552	−0.337	0.829	1.723	8.25%	0.89
	C	−0.042	1.093	−0.418	0.012	0.410	0.689	0.63%	0.98
e_a (Pa)	O	93.467	72.866	52.510	98.948	139.279	102.291	16.30%	0.88
	C	−0.078	31.798	−10.772	−0.072	10.442	18.887	0.01%	0.97
SW_{rad}	N[d]	3.603	4.225	0.087	2.413	6.501	4.008	41.13%	0.91
(MJ m^{-2} d^{-1})	S[e]	0.380	4.596	−2.284	−0.839	2.742	3.461	4.34%	0.84
LAI (m^2 m^{-2})		0	0.587	−0.222	0.017	0.299	0.404	0	0.91
FPAR		0	0.070	−0.030	0.005	0.040	0.050	0	0.93

[a]The statistics include mean ($\bar{\varepsilon}$), median (M_{ε}), standard deviation (i.e., standard error, s_{ε}), first quartile (Q_1), and third quartile (Q_3) of the error distribution, mean absolute error (MAE), relative error (δ), and correlation between estimated and "true" values (i.e., daily weather station observations and MODIS FPAR/LAI time series).
[b]O indicates the original NNR reanalysis meteorology.
[c]C indicates the corrected NNR reanalysis meteorology.
[d]N indicates the NNR reanalysis.
[e]S indicates the NASA/GEWEX SRB.

and SRB solar radiation products are also shown in Table 1. These results show considerable uncertainties in the original NNR meteorological data, especially for e_a. The original NNR shows substantial bias in mean errors for all three variables. Both T_{min} and T_{avg} are generally underestimated for the original NNR, while e_a is greatly overestimated. The mean errors of the three variables in the corrected NNR are near zero indicating that the corrected NNR should impart minimal bias to the NPP calculations. The quartile and median error statistics indicate that errors for all the three variables are slightly skewed, whereas errors in the corrected NNR show a normal distribution. The standard and mean absolute errors of these results indicate that the error spreads are greatly reduced by the corrections. Reductions in relative errors also indicate that the correction procedure has greatly improved accuracy of the NNR inputs. The correlation analysis also shows that correspondence between reanalysis and observations is greatly improved. These results indicate that the correction procedure effectively removed most uncertainties in NNR daily surface meteorological inputs relative to available surface weather station network observations.

[25] The maps of error spatial distributions of both NNR and corrected NNR T_{avg}, T_{min} and e_a inputs (Figure S1 in the auxiliary material[1]) indicate that errors in the original NNR have significant spatial patterns, while errors in the corrected NNR meteorology are negligible and without strong spatial patterns. Analyses of error temporal variation also indicate that the errors are negligible and temporally independent in the corrected NNR (Figure S2).

[26] Although both NNR and SRB solar radiation data are overestimated relative to the 17 station observation series, the mean error of SRB solar radiation is near zero and much smaller than the NNR product. The SRB error distribution spread is also much smaller than the NNR product. Although the NNR solar radiation has a somewhat higher correlation with the observations than the SRB, both the relative error and error spread statistics indicate that the SRB is more

accurate than the NNR solar radiation product for the study region. Temporal error analysis of SRB SW_{rad} (Figure S2) also indicates that the errors are small and temporally independent.

[27] The sensitivity and error propagation analyses are consistent with previous findings [*Zhang et al.*, 2007a] that NNR solar radiation is the primary source of PEM-based NPP uncertainty for the pan-Arctic region (Table 2). The use of SRB SW_{rad} instead of NNR SW_{rad} significantly ($P < 0.05$) reduced associated NPP estimation uncertainty for the two main biomes (Table 2). The correction of NNR T_{avg}, T_{min} and e_a also significantly ($P < 0.05$) decreased uncertainty in PEM based NPP calculations for the two main biomes (Table 2). Mean annual NPP for the region derived from corrected NNR and SRB inputs was overestimated by approximately 4.8%, which is much lower than relative error (61.6%) produced from NNR radiation inputs [*Zhang et al.*, 2007a].

[28] Since the simple linear regression method is unbiased, the mean error of the adjusted AVHRR FPAR/LAI series is zero relative to the MODIS FPAR/LAI product and there is no bias in the combined AVHRR-MODIS FPAR/LAI time series. The quartile and median statistics indicate that errors from the adjusted AVHRR FPAR/LAI series are normally distributed; standard and mean absolute error

Table 2. Comparison of Estimated Average Errors of Three PEM NPP Series Derived From the Following Meteorological Inputs: (1) Corrected NNR T_{avg}, T_{min} and e_a, and NASA/GEWEX SRB SW_{rad}; (2) Corrected NNR T_{avg}, T_{min} and e_a, and NNR SW_{rad}; (3) NNR T_{avg}, T_{min}, e_a, and SW_{rad} Using the Sensitivity Analysis Procedures of *Zhang et al.* [2007a][a]

Vegetation Type	Estimated Mean Errors of PEM NPP (g C m^{-2} a^{-1})		
	Driven by Meteorology Inputs 1	Driven by Meteorology Inputs 2	Driven by Meteorology Inputs 3
Boreal Forest	27.26(a)	351.10(b)	380.23(c)
Tundra	14.60(a)	171.58(c)	152.20(c)

[a]Different letters denote significant ($P < 0.05$, $n = 99$) differences between NPP errors derived from the different meteorology inputs according to the S-N-K ANOVA.

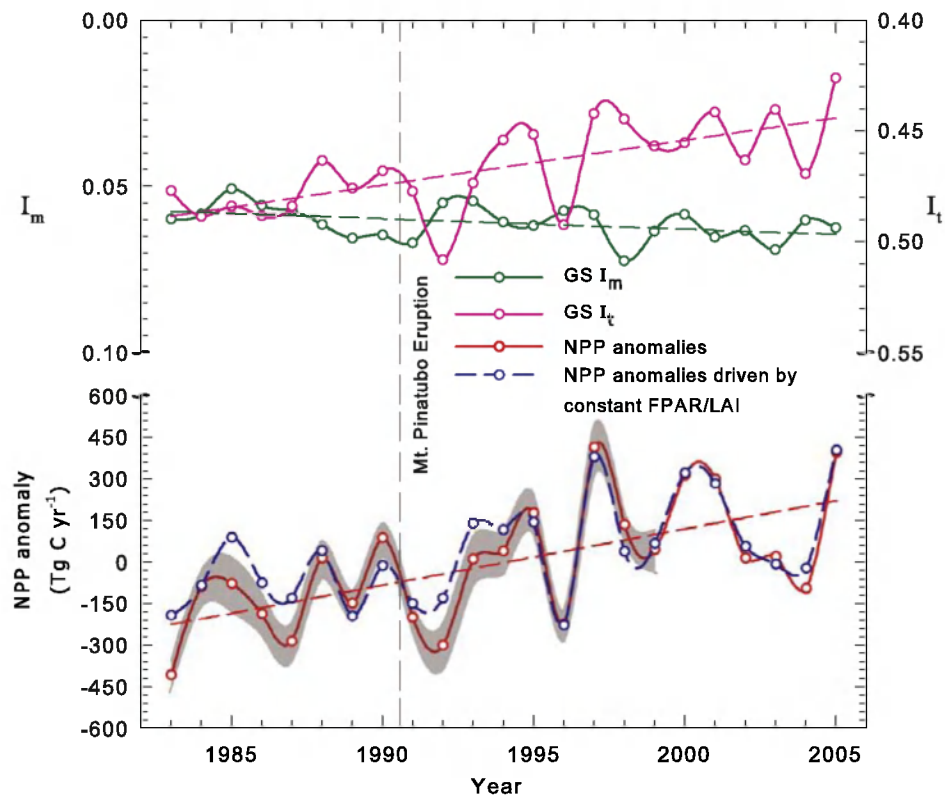[1]Auxiliary materials are available in the HTML. doi:10.1029/2007JG000621.

Figure 2. Annual NPP anomalies, mean growing season (GS, April–October) I_m and mean GS I_t from 1983 to 2005 for the pan-Arctic domain; the y axis for I_m and I_t increases from upper to lower portions of the graphic and corresponds to increasing environmental constraints on productivity. Linear trends for the three variables are shown as dotted lines. The 95% confidence intervals of estimated NPP before 2000 are also shown, and account for potential errors from the AVHRR-MODIS FPAR/LAI integration method. The NPP anomalies driven by constant FPAR/LAI are shown as the blue dash line.

statistics also show that the errors have a narrow spread. Correlation coefficients of 0.91 and 0.93 indicate strong correspondence between the adjusted AVHRR and MODIS FPAR/LAI series. Therefore, both error distribution and correlation analyses indicate that the approach for combining AVHRR and MODIS FPAR/LAI time series is reliable. Although errors from the adjusted AVHRR FPAR/LAI series show a slight spatial variation in 2000 (Figure S3), the errors are confined to a relatively small area and narrow intervals (± 0.4 m^2 m^{-2} for LAI; ± 0.06 for FPAR) over more than 90% of the vegetated domain.

[29] The narrow 95% confidence intervals of estimated NPP before 2000 (Figure 2) indicate that the methods for combining the AVHRR and MODIS time series are reliable and robust, and that potential FPAR/LAI errors do not introduce significant uncertainty into NPP calculations for the domain. The NPP results derived using constant FPAR/LAI inputs accounted for 86.13% ($P < 0.001$) of the variability in NPP results derived from the historical FPAR/LAI record (Figure 2), indicating that the observed pan-Arctic NPP trends are primarily climate driven rather than a response to changes in photosynthetic canopy cover. These results also indicate that uncertainties associated with the combined AVHRR-MODIS FPAR/LAI series have a relatively small impact on PEM based estimates of regional NPP trends and annual variability for the domain. These results are also consistent with analyses of previous NPP

series derived from AVHRR PAL FPAR/LAI inputs and NNR and ERA40 meteorological data for the overlapping period: 1983–2000 (Figure S4) [*Zhang et al.*, 2007a] in terms of capturing major annual anomalies and regional trends in surface meteorology and vegetation productivity.

3.2. Comparison Between PEM-Derived NPP and CIPHA Site Measurements

[30] Figure 3 shows the CIPHA stand inventory network derived mean boreal aspen growth observations from 1951 to 2004 and corresponding PEM based mean annual NPP anomalies from 1983 to 2004. Also shown are the major drought and defoliation years for the region as reported by *Hogg et al.* [2005]. The trend line using a best fitting quadratic equation is also shown, indicating a general increasing growth trend with large annual variations due to the effects of periodic insect defoliations, drought, and vegetation regrowth. It should be noted that the tree ring based growth estimates also reflect the normal process of stand development, e.g., age, mortality, and competition, though annual growth variations have been linked to the effects of climate and insects [*Hogg et al.*, 2005].

[31] The PEM based annual NPP anomalies were positively correlated ($r = 0.56$; $P = 0.007$) with mean stand-level observations of boreal aspen growth for the 72 CIPHA sites. Both the PEM and CIPHA time series showed large decreases in plant growth in 1995, 1998, 2002, and 2003.
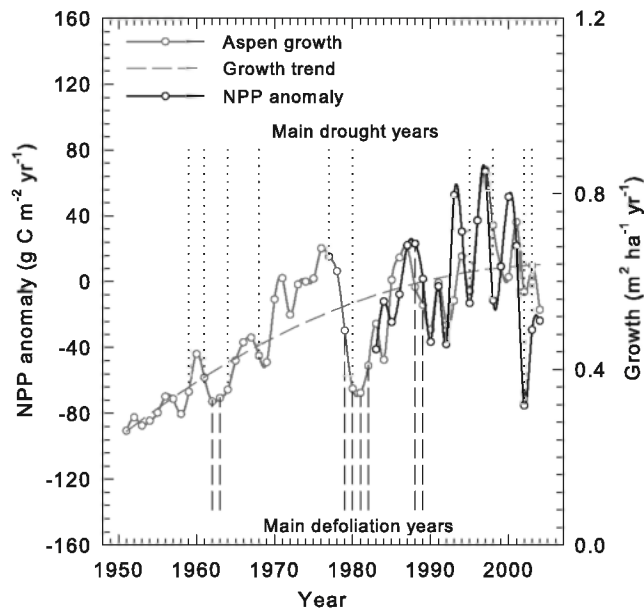
Figure 3. Comparison between PEM-derived NPP anomalies and boreal aspen growth derived from tree ring analyses for 72 CIPHA stands across western Canada. Vertical dotted lines and dashed lines denote major drought and insect defoliation years, respectively, as reported by *Hogg et al.* [2005].

These anomalous productivity declines have been attributed to severe regional drought conditions for these years [*Hogg et al.*, 2005]. Both data series confirm a generally positive vegetation growth trend for the 1980s and 1990s (1.65% per year, $P = 0.03$ for CIPHA Aspen growth; 0.67% per year, $P = 0.07$ for PEM derived NPP) and recent drought-induced NPP decreases after late-1990s.

3.3. Spatial Patterns and Temporal Anomalies of NPP Changes

[32] The integrated mean annual NPP results for the pan-Arctic domain showed a positive linear productivity trend of 0.34% per year (20.27 TgC/a; $P = 0.002$) from 1983 to 2005 (Figure 2). The generally increasing NPP trend during the 23-year period is mainly driven by a declining trend (-0.43% per year; $P < 0.001$) in low-temperature stress (I_t) during the growing season (April–October), defined as all months in which the 1983–2005 monthly average temperature for the pan-Arctic domain is above 0.0°C. However, a coincident and strong increasing trend (0.49% per year; $P = 0.04$) in growing season moisture stress (I_m) partially counteracts the positive effects of more favorable temperatures for photosynthesis. The larger magnitude of I_t relative to I_m (Figure 2) indicates that low temperature during the growing-season is generally the dominant limiting factor for NPP in the pan-Arctic domain. The integrated NPP series also captured large regional productivity decreases in 1991 and 1992, which have been attributed to temporary global cooling following the Mount Pinatubo eruption in June 1991 [*Luhr*, 1991; *Lucht et al.*, 2002]. Earlier onset and lengthening of growing seasons with regional warming are also potential drivers of positive NPP trends [*McDonald et al.*, 2004; *Kimball et al.*, 2006c]. The strong correlation ($r = 0.78$; $P < 0.001$)

between *NPP* and atmospheric CO_2 observation derived estimates of growing season onset (Figure 4) indicates that the PEM captures the annual timing and generally earlier arrival of the growing season with regional warming. Both of these data sets indicate a small, but insignificant advancing trend of 1.3–1.7 d per decade in average annual onset of the growing season.

[33] There was considerable spatial variability in NPP anomalies and trends, and associated moisture (I_m) and temperature (I_t) constraints to productivity (Table 3). For tundra, the PEM results showed a positive NPP trend (0.50% per year, $P < 0.001$) that was primarily driven by a declining trend in I_t (-0.41% per year, $P < 0.001$), indicating a relaxation of the low temperature constraint to productivity. The tundra biome showed positive, but insignificant trends in I_m, indicating that moisture limitations are increasing with regional warming but are not yet a major influence on tundra NPP trends. For the boreal forest biome, annual NPP showed a weak, positive trend (0.20% per year) over the long-term record. The I_t results for this region showed a strong decreasing trend (-0.49% per year, $P < 0.01$) for the period, which coincided with a significant negative trend in the associated moisture constraint to NPP. The results summary in Figure 5 shows that the low-temperature constraint to productivity is relaxing over the 23-year period, leading to less potential NPP loss for the two biomes, whereas the moisture constraint is increasing and partially counteracting the potential benefits of warmer temperatures. Over the long-term record, moisture constraints reduce annual NPP by 10.11% relative to potential conditions for the pan-Arctic region. This relative annual NPP reduction increased from 9.51% in the 1980s to 11.16% after 2000. Annual productivity for tundra appears to benefit much more from the warming trend and suffers
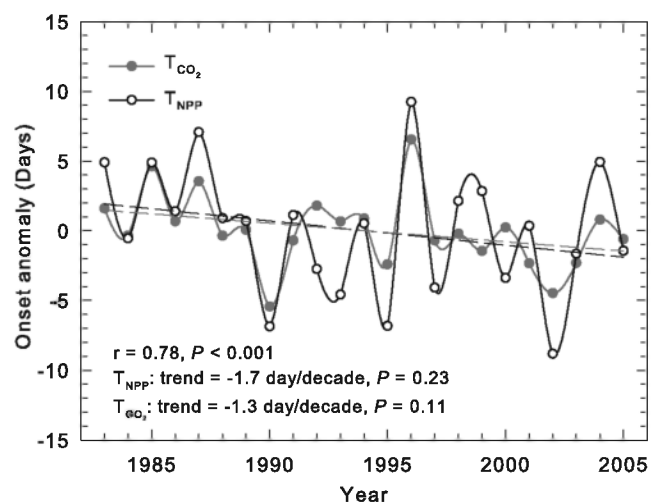

Figure 4. Correspondence ($r = 0.78$; $P < 0.001$) between annual anomalies of regional average growing season onset (T_{NPP}) defined by the timing of five of seven consecutive days with positive daily *NPP* values and the timing of the spring drawdown of atmospheric CO_2 (T_{CO2}) from NOAA GMD high-latitude (>50°N) monitoring sites; negative anomalies denote earlier onset of the growing season, while positive values denote the opposite response relative to the 23-year record.
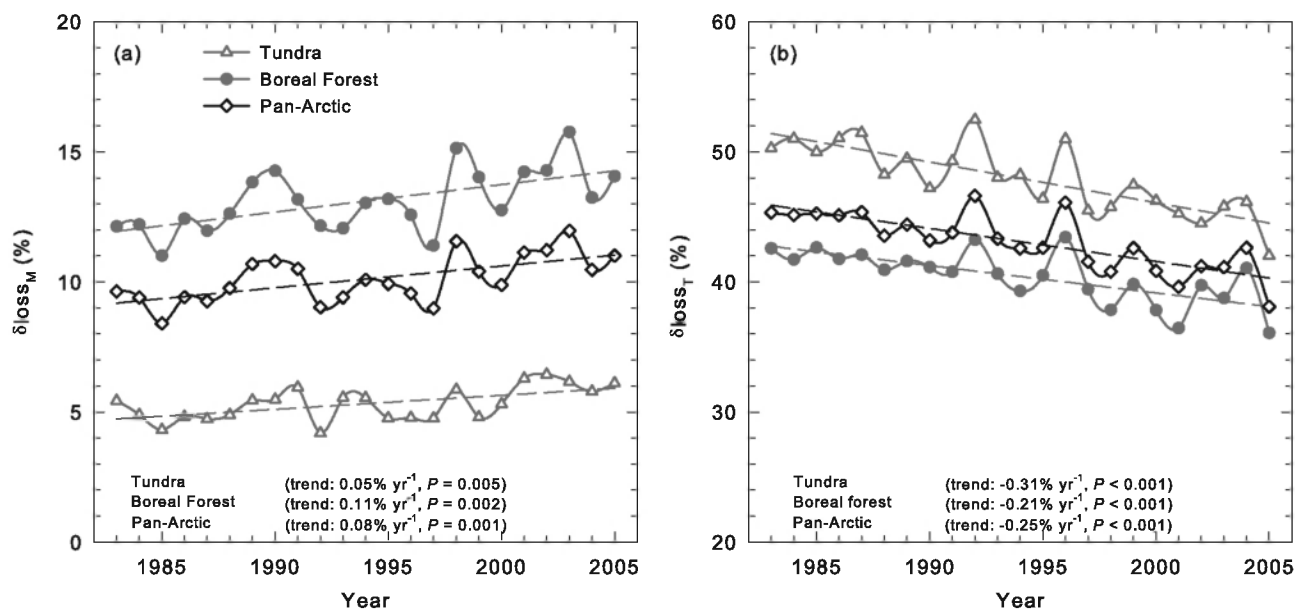
Figure 5. Proportional losses of potential NPP due to (a) moisture ($\delta loss_M$) and (b) low-temperature ($\delta loss_T$) constraints for the three major land cover types within the entire pan-Arctic domain. The dashed lines denote linear trends.

less from moisture limitations; tundra is mainly temperature limited, with average 47.96% and 5.32% losses relative to potential conditions due to low-temperature and moisture constraints, respectively. Boreal forests show a strong moisture constraint to productivity, resulting in a significant increasing trend in drought related NPP losses (0.11% per year; $P = 0.002$). However, the warming trend also reduces low temperature constraints to productivity for boreal forest as indicated by a decreasing trend in low temperature related losses in potential NPP of -0.21% per year ($P < 0.001$).

[34] The Figure 5 summary also shows that relatively cool conditions in 1992, 1996 and 2004, and periodic dry conditions from 1989 to 1991, 1998–1999, and 2001–2003 coincided with large NPP declines for the pan-Arctic region, as shown in Figure 2. Our results (Figure 5) indicate three major drought periods for the pan-Arctic region from 2001 to 2003, 1998–1999, and 1989–1991, which are ranked in terms of highest to lowest relative severity of potential NPP losses due to moisture limitations. These drought events are confirmed by mean annual CMI anomalies derived from the regional surface weather station network (Figure 6). The CMI shows a drying trend of -2.73 mm/a ($P < 0.001$) from

1974 to 2005 for the domain. The relative strength of the negative CMI anomalies and proportional losses of potential NPP from increasing I_m based constraints after 2000 indicates that the severity and persistence of the post-2000 drought is unprecedented for the 30+ year station record. These conditions also promoted a widespread NPP decline relative to potential conditions for the domain (Figure 2).

[35] The spatial patterns of summer I_m and annual NPP anomalies for 1998, 2001, 2002, and 2003 are presented in Figure 7. These results indicate summer drought across much of the domain with corresponding decreases in annual
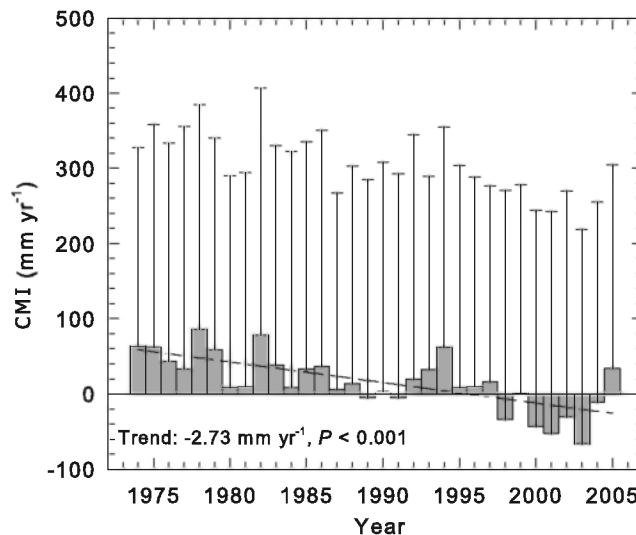

Table 3. Summary of Annual NPP Trend and Growing Season (April–October) Atmospheric Moisture Stress (I_m) and Low Temperature Stress (I_t) Indices Within the Study Domain for Tundra and Boreal Forest[a]

	NPP Trend		I_m		I_t	
Land Cover	Trend (% a^{-1})	Mean (Tg C)[b]	Trend (% a^{-1})	Mean	Trend (% a^{-1})	Mean
Tundra	0.50***	2288.79	0.34	0.030	-0.41***	0.543
Boreal forest	0.20	3364.90	0.59*	0.085	-0.49**	0.405

[a]Positive trends in I_m and I_t indicate increasing moisture and low temperature constraints to NPP, respectively, while negative trends denote the opposite response. *$P < 0.05$, **$P < 0.01$, ***$P < 0.001$.
[b]Mean is the 23-year mean.

Figure 6. Mean annual climate moisture index (CMI, $P - PET$) for the pan-Arctic basin and Alaska domain and 1974–2005 period; error bars denote the standard deviation of annual observations for the domain. The total number of NCDC CSB stations used to compute the index ranged from 2053 to 2924 per year.
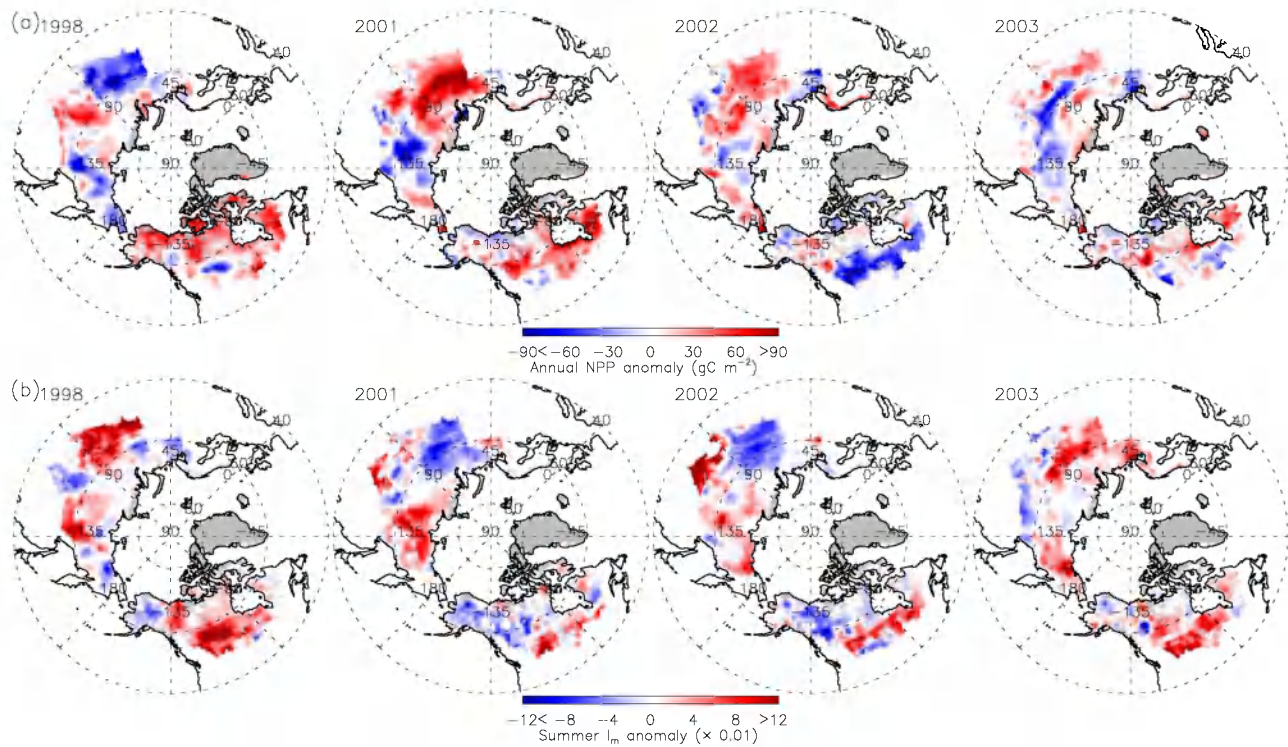
Figure 7. Maps of annual NPP and summer (June–August) I_m anomalies (relative to the 23-year mean) for 1998, 2001, 2002, and 2003. A positive anomaly for I_m corresponds to increasing moisture constraints on productivity relative to the long-term mean.

NPP. Summer (June–August) drought, indicated by anomalous increases in I_m, contributed to reductions in PEM derived annual NPP for predominantly inland areas including western and central Canada and southern and central Eurasia. Model results for eastern Alaska also indicated widespread drought effects. These results are consistent with the timing and location of recent documented drought events. *Waple et al.* [2002] reported that Canada experienced one of its most serious and extensive droughts on record in 2001, while the most severely affected areas occurred in the Canadian Prairies where the 2001 drought followed two to three consecutive years of below-average rainfall. *Waple et al.* [2003] also reported that some areas of central Canada suffered the driest August on record and western Canada suffered the second consecutive year with the most severe drought on record in 2002. Alaska had the warmest recorded year to date in 2002, while Russia reported a substantial precipitation deficit in July and August of 2002, which led to meteorological and hydrological drought for most of the region. In 2003, drier-than-normal conditions continued in the western provinces despite relatively wet conditions in other regions of Canada [*Levinson et al.*, 2004]; during July, anomalously warm and dry conditions appeared in some regions of Eurasia.

4. Discussion and Conclusions

[36] The PEM based NPP results may be negatively impacted by uncertainties in satellite remote sensing inputs including the PAL FPAR/LAI product, which incorporates uncertainties from dropped scan lines, navigation errors, data drop outs, edge-of-orbit composite discontinuities, and other artifacts of the AVHRR NDVI series [*Cihlar et al.*, 1997; *Tucker et al.*, 2005]. The NASA GIMMS NDVI product has attempted to correct most of the above problems and is currently available at 8-km resolution [*Pinzon et al.*, 2004]. However, there is currently no alternative GIMMS FPAR/LAI product with similar spatial resolution to the 16-km PAL data set. Though the SRB solar radiation product is of generally good quality, solar radiation has a larger uncertainty relative to the other PEM inputs for the domain. Therefore, the solar radiation inputs may introduce uncertainty into the PEM calculations. However, the impact of these uncertainties on NPP calculations is partially mitigated by the relative importance of other surface meteorological inputs to the PEM.

[37] Despite the potential negative effects of the above uncertainties, the generally consistent temporal patterns between PEM derived NPP and tree ring based aspen growth observations (Figure 3) indicate that the NPP time series from relatively coarse resolution satellite remote sensing effectively captures the regional impacts of summer drought, along with the impacts of transient global cooling following a major volcanic eruption. Both stand inventory observations and satellite based PEM results also confirm a generally positive vegetation growth trend for the 1980s and 1990s across west-central Canada and recent drought-induced NPP decreases after the late 1990s.

[38] Our results show that increasing productivity trends generally occur in tundra regions while NPP reductions occur in boreal forest regions. These findings are consistent with previous AVHRR GIMMS based analyses of regional photosynthetic trends [*Goetz et al.*, 2005; *Bunn and Goetz*, 2006]. Our results also indicate that recent widespread NPP

reductions in boreal forest regions were due to vegetation drought stress, which is also consistent with previous studies of AVHRR-based photosynthetic trends [*Bunn and Goetz*, 2006; *Goetz et al.*, 2007]. The negative effects of recent drought on terrestrial productivity are widespread for boreal regions, impacting not only western and central Canada but also eastern Alaska and south-central Eurasia. These results are also supported by other published field observations. In Alaska, tree ring studies showed a reduction in the growth of white spruce [*Barber et al.*, 2000, 2004; *Davi et al.*, 2003], even at some upper tree line sites [*Lloyd and Fastie*, 2003; *Wilmking et al.*, 2004], because of a recent increase in temperature-induced drought stress. *Hogg and Wein* [2005] also reported the negative impacts of recent drought on forest growth and regeneration in southwestern Yukon, Canada.

[39] Over western and central Canada, most available moisture for precipitation comes from the Pacific Ocean in winter (November–March) and the Gulf of Mexico in summer (May–August) [*Liu et al.*, 2004]. Thus regional precipitation has strong teleconnections to global sea surface temperature (SST) patterns [*Shabbar and Skinner*, 2004], especially variations in tropical and north Pacific SSTs [*Seager et al.*, 2005; *Zhang et al.*, 2007b], which may explain the relative persistence of recent drought in southern Alaska and southwestern Eurasia. *Goetz et al.* [2007] reported the lagged correlation between spring climate fields (like temperature and precipitation) and spring boreal North America net carbon exchange and suggested teleconnections between carbon fluxes in the pan-arctic region and large-scale atmospheric/oceanic oscillations such as the Arctic Oscillation and ENSO. More explicit analyses of teleconnections between climate oscillations and pan-Arctic NPP patterns were also documented by *Zhang et al.* [2007b]. The results of this study show that the largest negative NPP anomalies are predominantly located in relatively drought prone inland areas with greater annual extremes in temperature and precipitation. In addition, earlier spring thawing and corresponding earlier and longer growing seasons in this region [*McDonald et al.*, 2004; *Kimball et al.*, 2006c; *Waple et al.*, 2002, 2003; *Levinson et al.*, 2004] may be contributing to drought by enhancing vegetation growth and potential water loss. *Bunn and Goetz* [2006] reported that the recent boreal browning trends are more pronounced in more densely forested areas, as derived from MODIS tree cover products, which may reflect a greater vegetation water use requirement and potential drought stress for these areas.

[40] Future changes in terrestrial productivity will depend strongly on adequate supplies of plant-available moisture to support positive vegetation growth trends under a warming climate. Positive trends in regional warming and drying (Figure 2), and earlier onset of the growing season (Figure 4), are consistent with previous studies. Current and projected future warming of the region with a declining or negative water balance (i.e., the difference between precipitation and evaporation) will likely result in more frequent and severe drought, leading to further decreases in regional productivity and impairing the potential terrestrial sink strength for atmospheric CO_2. However, regional warming with commensurate increases in precipitation and a positive water balance [*Cassano et al.*, 2007] will likely support further increases in productivity. In addition, future warming likely surpasses the photosynthetic temperature optimum of many boreal tree species such as black spruce [*Way and Sage*, 2008], reducing forest carbon sequestration and altering associated species composition in this region. However, our results also indicate that in tundra biomes the relaxation of low-temperature constraints to photosynthesis is still the dominant environmental factor driving positive NPP trends despite concurrent increases in plant available moisture constraints. These results are consistent with AVHRR GIMMS based observations of positive photosynthetic trends for North American tundra [*Goetz et al.*, 2005]. The observed regional trajectory in I_m indicates that the negative effects of increasing moisture constraints on productivity are likely to become more severe and widespread under a warming climate, counteracting the positive effects of a lengthening growing season, without sufficient increases in precipitation to offset increasing evapotranspiration demands. Improvements in the spatial resolution of regional climate reanalyses coupled with standardization and augmentation of solar radiation and precipitation monitoring networks, and enhanced resolution satellite remote sensing products would dramatically improve the regional assessment of NPP changes and associated linkages between the terrestrial water and carbon cycles.

References

Angert, A., et al. (2005), Drier summers cancel out the CO_2 uptake enhancement induced by warmer springs, *Proc. Natl. Acad. Sci. U. S. A.*, *102*, 10,823–10,827, doi:10.1073/pnas.0501647102.

Arctic Climate Impact Assessment (ACIA) (2004), *Impacts of a Warming Arctic*, 146 pp., Cambridge Univ. Press, Cambridge, UK.

Barber, V. A., G. P. Juday, and B. P. Finney (2000), Reduced growth of Alaskan white spruce in the twentieth century from temperature-induced drought stress, *Nature*, *405*, 668–673, doi:10.1038/35015049.

Barber, V. A., G. P. Juday, B. P. Finney, and M. Wilmking (2004), Reconstruction of summer temperatures in interior Alaska from tree-ring proxies: Evidence from changing synoptic climate regimes, *Clim. Change*, *63*, 91–120, doi:10.1023/B:CLIM.0000018501.98266.55.

Bunn, A. G., and S. J. Goetz (2006), Trends in satellite-observed circumpolar photosynthetic activity from 1982 to 2003: The influence of seasonality, cover type, and vegetation density, *Earth Interact.*, *10*, 1–20, doi:10.1175/EI190.1.

Cassano, J. J., P. Uotila, A. H. Lynch, and E. N. Cassano (2007), Predicted changes in synoptic forcing of net precipitation in large arctic river basins during the 21st century, *J. Geophys. Res.*, *112*, G04S49, doi:10.1029/2006JG000332.

Cihlar, J., H. Ly, Z. Li, J. M. Chen, H. Pokrant, and F. Huang (1997), Multitemporal multichannel AVHRR data sets for land biosphere studies-artifacts and corrections, *Remote Sens. Environ.*, *60*, 35–57, doi:10.1016/S0034-4257(96)00137-X.

Davi, N. K., G. C. Jacoby, and G. C. Wiles (2003), Boreal temperature variability inferred from maximum latewood density and tree-ring width data, Wrangell Mountain region, Alaska, *Quat. Res.*, *60*, 252–262, doi:10.1016/j.yqres.2003.07.002.

Erickson, D. J., P. J. Rasch, P. P. Tans, P. Friedlingstein, P. Ciais, E. Maier-Reimer, K. Six, C. A. Fischer, and S. Walters (1996), The seasonal cycle

of atmospheric CO_2: A study based on the NCAR Community Climate Model (CCM2), *J. Geophys. Res.*, *101*, 15,079–15,097, doi:10.1029/95JD03680.

Euskirchen, E. S., et al. (2006), Importance of recent shifts in soil thermal dynamics on growing season length, productivity, and carbon sequestration in terrestrial high-latitude ecosystems, *Global Change Biol.*, *12*, 731–750, doi:10.1111/j.1365-2486.2006.01113.x.

Friedl, M. A., et al. (2002), Global land cover mapping from MODIS: Algorithms and early results, *Remote Sens. Environ.*, *83*(1–2), 287–302, doi:10.1016/S0034-4257(02)00078-0.

GLOBALVIEW-CO_2 (2006), *Cooperative Atmospheric Data Integration Project-Carbon Dioxide* [CD-ROM], Global Monit. Div., Natl. Oceanic and Atmos. Admin., Boulder, Colo.

Goetz, S. J., A. G. Bunn, G. J. Fiske, and R. A. Houghton (2005), Satellite-observed photosynthetic trends across boreal North America associated with climate and fire disturbance, *Proc. Natl. Acad. Sci. U. S. A.*, *102*(38), 13,521–13,525, doi:10.1073/pnas.0506179102.

Goetz, S. J., M. C. Mack, K. R. Gurney, J. T. Randerson, and R. A. Houghton (2007), Ecosystem responses to recent climate change and fire disturbance at northern high latitudes: Observations and model results contrasting northern Eurasia and North America, *Environ. Res. Lett.*, *2*, 1–9, doi:10.1088/1748-9326/2/4/045031.

Gupta, S. K., D. P. Kratz, P. W. Stackhouse Jr., and A. C. Wilber (2001), The Langley Parameterized Shortwave Algorithm (LPSA) for surface radiation budget studies, *NASA TP-2001–211272*, 31 pp.

Heimann, M., et al. (1998), Evaluation of terrestrial carbon cycle models through simulations of the seasonal cycle of atmospheric CO_2: First results of a model intercomparison study, *Global Biogeochem. Cycles*, *12*, 1–24, doi:10.1029/97GB01936.

Heinsch, F. A., et al. (2003), *User's Guide: GPP and NPP (MOD17A2/A3) Products NASA MODIS Land Algorithm*, Univ. of Mont., Missoula, Mont.

Heinsch, F. A., et al. (2006), Evaluation of remote sensing based terrestrial productivity from MODIS using regional tower eddy flux network observations, *IEEE Trans. Geosci. Remote Sens.*, *44*(7), 1908–1925, doi:10.1109/TGRS.2005.853936.

Hogg, E. H. (1997), Temporal scaling of moisture and the forest-grassland boundary in western Canada, *Agric. For. Meteorol.*, *84*, 115–122, doi:10.1016/S0168-1923(96)02380-5.

Hogg, E. H., and R. W. Wein (2005), Impacts of drought on forest growth and regeneration following fire in southwestern Yukon, Canada, *Can. J. For. Res.*, *35*, 2141–2150, doi:10.1139/x05-120.

Hogg, E. H., J. P. Brandt, and B. Kochtubajda (2002), Growth and dieback of aspen forests in northwestern Alberta, Canada, in relation to climate and insects, *Can. J. For. Res.*, *32*, 823–832, doi:10.1139/x01-152.

Hogg, E. H., J. P. Brandt, and B. Kochtubajda (2005), Factors affecting interannual variation in growth of western Canadian aspen forests during 1951–2000, *Can. J. For. Res.*, *35*, 610–622, doi:10.1139/x04-211.

Hogg, E. H., J. P. Brandt, and M. Michaelian (2008), Impact of a regional drought on the productivity, dieback and biomass of western Canadian aspen forests, *Can. J. For. Res.*, *38*, 1373–1384, doi:10.1139/X08-001.

Kalnay, E., et al. (1996), The NMC/NCAR 40-year reanalysis project, *Bull. Am. Meteorol. Soc.*, *77*, 437–471, doi:10.1175/1520-0477(1996)077<0437:TNYRP>2.0.CO;2.

Keeling, C. D., J. F. S. Chin, and T. P. Whorf (1996), Increased activity of northern vegetation inferred from atmospheric CO2 measurements, *Nature*, *382*, 146–149, doi:10.1038/382146a0.

Kimball, J. S., M. Zhao, K. C. McDonald, and S. W. Running (2006a), Satellite remote sensing of terrestrial net primary production for the pan-Arctic basin and Alaska, *Mitig. Adapt. Strat. Global Change*, doi:10.1007/s11027-005-9014-5.

Kimball, J. S., et al. (2006b), Recent climate driven increases in vegetation productivity for the Western Arctic: Evidence of an acceleration of the northern terrestrial carbon cycle, *Earth Interact.*, *11*(4), 1–23, doi:10.1175/EI180.1.

Kimball, J. S., et al. (2006c), Spring thaw and its effect on northern terrestrial vegetation productivity observed from satellite microwave and optical remote sensing, *Earth Interact.*, *10*(21), 1–22, doi:10.1175/EI187.1.

Kistler, R., et al. (2001), The NCEP/NCAR 50-year reanalysis: Monthly means CD-ROM and documentation, *Bull. Am. Meteorol. Soc.*, *82*, 247–268, doi:10.1175/1520-0477(2001)082<0247:TNNYRM>2.3.CO;2.

Lal, R., and J. M. Kimble (2000), Soil C pool and dynamics in cold ecoregions, in *Advances in Soil Science: Global Climate Change and Cold Regions Ecosystems*, edited by R. Lal, J. M. Kimble, and B. A. Steward, pp. 3–28, Lewis, New York.

Levinson, D. H., et al. (2004), State of the climate in 2003, *Bull. Am. Meteorol. Soc.*, *85*(6), S1–S72, doi:10.1175/BAMS-85-6-Levinson.

Liu, J., R. E. Stewart, and K. K. Szeto (2004), Moisture transport and other hydrometeorological features associated with the severe 2000/1 drought

over the western and central Canadian prairies, *J. Clim.*, *17*, 305–319, doi:10.1175/1520-0442(2004)017<0305:MTAOHF>2.0.CO;2.

Lloyd, A. H., and C. L. Fastie (2003), Recent changes in treeline forest distribution and structure in interior Alaska, *Ecoscience*, *10*, 176–185.

Lucht, W., et al. (2002), Climatic control of the high-latitude vegetation greening trend and Pinatubo effect, *Science*, *296*, 1687–1689, doi:10.1126/science.1071828.

Luhr, J. F. (1991), Volcanic shade causes cooling (Mount Pinatubo), *Nature*, *354*, 104, doi:10.1038/354104a0.

McDonald, K. C., J. S. Kimball, E. Njoku, R. Zimmermann, and M. Zhao (2004), Variability in springtime thaw in the terrestrial high latitudes: Monitoring a major control on the biospheric assimilation of atmospheric CO_2 with spaceborne microwave remote sensing, *Earth Interact.*, *8*(20), 1–23, doi:10.1175/1087-3562(2004)8<1:VISTIT>2.0.CO;2.

McGuire, A. D., et al. (2001), Carbon balance of the terrestrial biosphere in the twentieth century: Analysis of CO2, climate and land use effects with four process-based ecosystem models, *Global Biogeochem. Cycles*, *15*, 183–206, doi:10.1029/2000GB001298.

Myneni, R. B., C. D. Keeling, C. J. Tucker, G. Asrar, and R. R. Nemani (1997a), Increased plant growth in the northern high latitudes from 1981 to 1991, *Nature*, *386*, 698–702, doi:10.1038/386698a0.

Myneni, R. B., R. R. Nemani, and S. W. Running (1997b), Estimation of global leaf area index and absorbed par using radiative transfer models, *IEEE Trans. Geosci. Remote Sens.*, *35*, 1380–1393, doi:10.1109/36.649788.

Myneni, R. B., et al. (2002), Global products of vegetation leaf area and fraction absorbed PAR from year one of MODIS data, *Remote Sens. Environ.*, *83*, 214–231, doi:10.1016/S0034-4257(02)00074-3.

Nemani, R. R., C. D. Keeling, H. Hashimoto, W. M. Jolly, S. C. Piper, C. J. Tucker, R. B. Myneni, and S. W. Running (2003), Climate-driven increases in global terrestrial net primary production from 1982 to 1999, *Science*, *300*, 1560–1563, doi:10.1126/science.1082750.

Oechel, W. C., G. L. Vourlities, S. J. Hastings, and S. A. Bochkarev (1995), Change in arctic CO_2 flux over two decades: Effects of climate change at Barrow, Alaska, *Ecol. Appl.*, *5*, 846–855, doi:10.2307/1941992.

Oechel, W. C., G. L. Vourlities, S. J. Hastings, R. M. Zulueta, L. D. Hinzman, and D. K. Kane (2000), Acclimation of ecosystem CO_2 exchange in the Alaskan Arctic in response to decadal climatic warming, *Nature*, *406*, 978–981, doi:10.1038/35023137.

Oelke, C., T. Zhang, and M. C. Serreze (2004), Modeling evidence for recent warming of the arctic soil thermal regime, *Geophys. Res. Lett.*, *31*, L07208, doi:10.1029/2003GL019300.

Pinzon, J., M. E. Brown, and C. J. Tucker (2004), Satellite time series correction of orbital drift artifacts using empirical mode decomposition, in *Hilbert-Huang Transform: Introduction and Applications*, edited by N. E. Huang, pp. 173–176, NASA Goddard Space Flight Cent., Greenbelt, Md.

Randerson, J. T., C. B. Field, I. Y. Fung, and P. P. Tans (1999), Increases in early season ecosystem uptake explain recent changes in the seasonal cycle of atmospheric CO_2 at high northern latitudes, *Geophys. Res. Lett.*, *26*(17), 2765–2768, doi:10.1029/1999GL900500.

Running, S. W., P. E. Thornton, R. R. Nemani, and J. M. Glassy (2000), Global terrestrial gross and net primary productivity from the Earth Observing System, in *Methods in Ecosystem Science*, edited by O. E. Sala, R. B. Jackson, H. A. Mooney, and R. W. Howarth, pp. 44–57, Springer, New York.

Running, S. W., R. R. Nemani, F. A. Heinsch, M. Zhao, M. Reeves, and H. Hashimoto (2004), A continuous satellite-derived measure of global terrestrial primary productivity, *BioScience*, *54*(6), 547–560, doi:10.1641/0006-3568(2004)054[0547:ACSMOG]2.0.CO;2.

Saugier, B., J. Roy, and H. A. Mooney (2001), Estimations of global terrestrial productivity: Converging toward a single number?, in *Terrestrial Global Productivity*, edited by B. Saugier, J. Roy, and H. A. Mooney, pp. 543–557, Academic, San Diego, Calif.

Schindler, D. W., and W. F. Donahue (2006), An impending water crisis in Canada's western prairie provinces, *Proc. Natl. Acad. Sci. U. S. A.*, *103*, 7210–7216, doi:10.1073/pnas.0601568103.

Seager, R., Y. Kushnir, C. Herweijer, N. Naik, and J. Velez (2005), Modeling of tropical forcing of persistent droughts and pluvials over western North America: 1856–2000, *J. Clim.*, *18*, 4065–4088, doi:10.1175/JCLI3522.1.

Shabbar, A., and W. Skinner (2004), Summer drought patterns in Canada and the relationship to global sea surface temperature, *J. Clim.*, *17*, 2866–2880, doi:10.1175/1520-0442(2004)017<2866:SDPICA>2.0.CO;2.

Slayback, D. A., J. E. Pinzon, S. O. Los, and C. J. Tucker (2003), Northern hemisphere photosynthetic trends 1982–1999, *Global Change Biol.*, *9*, 1–15, doi:10.1046/j.1365-2486.2003.00507.x.

Stocks, B. J., et al. (2002), Large forest fires in Canada, 1959–1997, *J. Geophys. Res.*, *107*, 8149, doi:10.1029/2001JD000484 [printed *108*(D1), 2003].

Sturm, M., C. Racine, and K. Tape (2001), Increasing shrub abundance in the Arctic, *Nature*, *411*, 546–547, doi:10.1038/35079180.

Tucker, C. J., et al. (2005), An extended AVHRR 8-km NDVI data set compatible with MODIS and SPOT vegetation NDVI data, *Int. J. Remote Sens.*, *26*(20), 4485–4498, doi:10.1080/01431160500168686.

Turner, D. P., et al. (2003), Scaling gross primary production (GPP) over boreal and deciduous forest landscapes in support of MODIS GPP product validation, *Remote Sens. Environ.*, *88*, 256–270, doi:10.1016/j.rse.2003.06.005.

Turner, D. P., et al. (2005), Site-level evaluation of satellite-based global terrestrial gross primary production and net primary production monitoring, *Global Change Biol.*, *11*(4), 666–684, doi:10.1111/j.1365-2486.2005.00936.x.

Waple, A. M., et al. (2002), Climate assessment for 2001, *Bull. Am. Meteorol. Soc.*, *83*(6), S1–S62, doi:10.1175/1520-0477(2002)083<0938:CAF>2.3.CO;2.

Waple, A. M., et al. (2003), State of the climate in 2002, *Bull. Am. Meteorol. Soc.*, *84*(6), S1–S68, doi:10.1175/BAMS-84-6-Waple.

Way, D. A., and R. F. Sage (2008), Elevated growth temperatures reduce the carbon gain of black spruce, *Global Change Biol.*, *14*, 624–636, doi:10.1111/j.1365-2486.2007.01513.x.

White, M. A., P. E. Thornton, S. W. Running, and R. R. Nemani (2000), Parameterization and sensitivity analysis of the BIOME-BG C terrestrial ecosystem model: Net primary production controls, *Earth Interact.*, *4*(3), 1–85, doi:10.1175/1087-3562(2000)004<0003:PASAOT>2.0.CO;2.

Wilmking, M., G. P. Juday, V. Barber, and H. Zald (2004), Recent climate warming forces contrasting growth responses of white spruce at treeline in Alaska through temperature thresholds, *Global Change Biol.*, *10*, 1724–1736, doi:10.1111/j.1365-2486.2004.00826.x.

Zhang, K., J. S. Kimball, M. Zhao, W. C. Oechel, J. Cassano, and S. W. Running (2007a), Sensitivity of pan-Arctic terrestrial net primary productivity simulations to daily surface meteorology from NCEP-NCAR and ERA-40 reanalyses, *J. Geophys. Res.*, *112*, G01011, doi:10.1029/2006JG000249.

Zhang, K., J. S. Kimball, K. C. McDonald, J. J. Cassano, and S. W. Running (2007b), Impacts of large-scale oscillations on pan-Arctic terrestrial net primary production, *Geophys. Res. Lett.*, *34*, L21403, doi:10.1029/2007GL031605.

Zhao, M., F. A. Heinsch, R. R. Nemani, and S. W. Running (2005), Improvements of the MODIS terrestrial gross and net primary production global data set, *Remote Sens. Environ.*, *95*, 164–176, doi:10.1016/j.rse.2004.12.011.

Zhao, M., S. W. Running, and R. R. Nemani (2006), Sensitivity of Moderate Resolution Imaging Spectroradiometer (MODIS) terrestrial primary production to the accuracy of meteorological reanalysis, *J. Geophys. Res.*, *111*, G01002, doi:10.1029/2004JG000004.

Zhao, M., S. W. Running, F. A. Heinsch, and R. R. Nemani (2008), Terrestrial primary production from MODIS, in *Land Remote Sensing and Global Environmental Change: NASA's EOS and the Science of ASTER and MODIS*, edited by C. Justice and M. Abrams, Springer, New York.

Zhou, L., C. J. Tucker, R. K. Kaufmann, D. Slayback, N. V. Shabanov, and R. B. Myneni (2001), Variations in northern vegetation activity inferred from satellite data of vegetation index during 1981 to 1999, *J. Geophys. Res.*, *106*(D17), 20,069–20,084, doi:10.1029/2000JD000115.

J. J. Cassano, Cooperative Institute for Research in Environmental Sciences and Department of Atmospheric and Oceanic Sciences, University of Colorado, Boulder, CO 80309-0216, USA.

E. H. Hogg, Northern Forestry Centre, Canadian Forest Service, Natural Resources Canada, 5320-122 Street, Edmonton, AB T6H 3S5, Canada.

J. S. Kimball and K. Zhang, Flathead Lake Biological Station, University of Montana, 32125 Bio Station Lane, Polson, MT 59860-9659, USA. (zhang@ntsg.umt.edu)

W. C. Oechel, Global Change Research Group, Biology Department, San Diego State University, 5500 Campanile Drive, San Diego, CA 92182, USA.

S. W. Running and M. Zhao, Numerical Terradynamic Simulation Group, Department of Ecosystem and Conservation Sciences, University of Montana, 32 Campus Drive #1224, Missoula, MT 59812-1224, USA.